Vietnam Journal of Mechanics, VAST, Vol. 43, No. 4 (2021), pp. 319 – 331
DOI: https://doi.org/10.15625/0866-7136/16152

A 4-NODE QUADRILATERAL ELEMENT WITH CENTER-POINT BASED DISCRETE SHEAR GAP (CP-DSG4)

Minh Ngoc Nguyen[1,*], **Tinh Quoc Bui**[2], **Vay Siu Lo**[3,4], **Nha Thanh Nguyen**[3,4]
[1]*Duy Tan Research Institute for Computational Engineering (DTRICE), Duy Tan University, Ho Chi Minh City, Vietnam*
[2]*Department of Civil and Environmental Engineering, Tokyo Institute of Technology, 2-12-1-W8-22, Ookayama, Meguro-ku, Tokyo 152-8552, Japan*
[3]*Department of Engineering Mechanics, Faculty of Applied Science, Ho Chi Minh City University of Technology (HCMUT), Vietnam*
[4]*Vietnam National University Ho Chi Minh City, Vietnam*
[*]E-mail: nguyenngocminh6@duytan.edu.vn

Received: 12 June 2021 / Published online: 20 October 2021

Abstract. This work aims at presenting a novel four-node quadrilateral element, which is enhanced by integrating with discrete shear gap (DSG), for analysis of Reissner–Mindlin plates. In contrast to previous studies that are mainly based on three-node triangular elements, here we, for the first time, extend the DSG to four-node quadrilateral elements. We further integrate the fictitious point located at the center of element into the present formulation to eliminate the so-called anisotropy, leading to a simplified and efficient calculation of DSG, and that enhancement results in a novel approach named as "four-node quadrilateral element with center-point based discrete shear gap - CP-DSG4". The accuracy and efficiency of the CP-DSG4 are demonstrated through our numerical experiment, and its computed results are validated against those derived from the three-node triangular element using DSG, and other existing reference solutions.

Keywords: discrete shear gap, four-node quadrilateral element, finite element method, Reissner–Mindlin plate theory, CP-DSG4.

1. INTRODUCTION

The Reissner–Mindlin theory, known as the first order shear deformation theory - FSDT, is popular and has been intensively used for investigating plate structures. In terms of numerical simulation, the theory only requires the shape functions to satisfy C^0-continuity, which is much more convenient than either the Kirchhoff theory for thin plates or higher-order shear deformation theories. Reissner–Mindlin theory is applicable for both moderately thick and thin plates, it however is suffered from the so-called *shear locking* problem in the sense of thin plates analysis. A simple remedy namely selective

reduced integration [1] may be used, i.e., less number of integration points than as usual are used for computation of the shear stiffness. However it is not versatile and thus, development of other treatments is necessary.

A large number of techniques have been proposed so far to treat the shear locking in the context of finite element method (FEM), i.e. various versions of the 8-node quadrilateral elements [2, 3], the family of MITC elements based on mixed formulation [4–6], the assumed strain [7, 8], etc. The technique of discrete shear gap, originally proposed by Bletzinger et al. [9] can also be considered as assumed strain, in which the shear gap is approximated from the nodal displacements, i.e. deflection and rotations. The formulation is quite straightforward, especially in the case of three-node triangular element. However, it is pointed out in [10] that the performance is dependent to the order of node sequence, which is called by "anisotropy". Recently, Cui et al. [11] proposed the introduction of a fictitious point located at the center of triangular element to eliminate the issue of "anisotropy" and thus improve the accuracy.

Alternatively to FEM, many other numerical methods were developed including isogeometric analysis (IGA) [12, 13], meshfree methods [14, 15], and smoothed FEM [3, 16]. Each method has its own advantages and disadvantages. In the IGA, the continuity and the order of the shape function is controllable, which is also effective to deal with the shear locking. However, the desirable property of Kronecker delta is lost, leading to difficulty in imposition of boundary conditions. Similarly, the meshfree methods in most of the cases possess higher order and higher continuity shape functions. Unfortunately, only a few types of meshfree methods, e.g. the Radial Point Interpolation Method, satisfy Kronecker delta. Nevertheless, computational time in meshfree analysis is generally higher than that of finite element analysis. The polygonal FEM and the smoothed FEM are improved versions of traditional FEM. In polygonal FEM, elements of polygonal shape being associated with higher order shape function are introduced to increase the accuracy. New techniques of discretization (namely meshing) are required accordingly. In the smoothed FEM, the compatible strain tensor is replaced by a smoothing strain tensor, resulting in better approximation, with the price of more complicated computation. In order to effectively mitigate the shear locking, the polygonal FEM and smoothed FEM still need to combine with techniques such as assumed strain [17] and discrete shear gap [16, 18].

In this paper, the discrete shear gap (DSG) is incorporated into four-node quadrilateral element, in order to alleviate shear locking and improve performance, while calculation is kept as simple as possible. It is noted that the DSG formulation proposed in [9] is applicable to four-node quadrilateral element. The element, namely DSG4, is reported in [9] to be equivalent to the element with assumed natural strain. However, the implementation was not mentioned in details. Being inspired by the work of Cui et al. [11] for three-node triangular elements, the current study also exploits the fictitious point to eliminate the so-called "anisotropy" and to achieve a simple calculation of DSG. Theoretically, the fictitious point can be any point within the element. However, selection of the center point would be convenient and helps to increase computational efficiency. Hence, the proposed element is named by "four-node quadrilateral element with center-point based discrete shear gap" (CP-DSG4).

2. BRIEF ON REISSNER-MINDLIN PLATE THEORY

According to the Reissner–Mindlin plate theory, the displacement fields $\left[u_x, u_y, u_z\right]^T$ at an arbitrary point can be estimated by

$$u_x(x,y,z) = -z\beta_x(x,y), \tag{1}$$

$$u_y(x,y,z) = -z\beta_y(x,y), \tag{2}$$

$$u_z(x,y,z) = w(x,y), \tag{3}$$

in which w is the vertical displacement at the mid-surface (namely deflection) and β_x, β_y are the rotations about y- and x-axes, respectively. The strain components are then obtained by

$$\text{Bending strains:} \quad \boldsymbol{\varepsilon}_b = \left[\varepsilon_{xx}, \varepsilon_{yy}, 2\varepsilon_{xy}\right]^T = \left[-z\beta_{x,x}, -z\beta_{y,y}, -z\left(\beta_{x,y} + \beta_{y,x}\right)\right]^T, \tag{4}$$

$$\text{Shear strains:} \quad \boldsymbol{\varepsilon}_s = \left[2\varepsilon_{xz}, 2\varepsilon_{yz}\right]^T = \left[w_{,x} - \beta_x, w_{,y} - \beta_y\right]^T. \tag{5}$$

The Galerkin weak form for static bending analysis of Reissner–Mindlin plates is given as follows:

$$\int_\Omega (\delta\boldsymbol{\varepsilon}^b)^T \mathbf{D}_b \boldsymbol{\varepsilon}^b \mathrm{d}\Omega + \int_\Omega (\delta\boldsymbol{\varepsilon}^s)^T \mathbf{D}_s \boldsymbol{\varepsilon}^s \mathrm{d}\Omega = \int_\Omega \delta\mathbf{u}^T \mathbf{b} \mathrm{d}\Omega, \tag{6}$$

where $\mathbf{u} = \left[w,\ \beta_x,\ \beta_y\right]^T$ is the vector of unknown displacement components; $\mathbf{b} = [q,\ 0,\ 0]$ is the vector of distributed load; and Ω is the plate domain.

For homogeneous and isotropic materials, the material matrices $\mathbf{D}_b$ and $\mathbf{D}_s$ characteristic for bending and shearing, respectively, are given by

$$\mathbf{D}_b = \frac{Et^3}{12\left(1-\nu^2\right)} \begin{bmatrix} 1 & \nu & 0 \\ \nu & 1 & 0 \\ 0 & 0 & \dfrac{1-\nu}{2} \end{bmatrix}, \tag{7}$$

$$\mathbf{D}_s = \kappa t \begin{bmatrix} \mu & 0 \\ 0 & \mu \end{bmatrix}. \tag{8}$$

In the above equations, the material parameters are the Young modulus E, the Poisson's ratio ν and the shear modulus $\mu = \dfrac{E}{2\left(1+\nu\right)}$, while t is the thickness of the plate. A shear correction factor $\kappa = \dfrac{5}{6}$ is usually taken in practice.

3. FORMULATION OF DISCRETE SHEAR GAP

3.1. Brief on existing implementation of DSG

The terminology of shear gap was introduced in [9] for a two-node Timoshenko beam element by integration of shear strain along the element, i.e.

$$v(x) = \int \varepsilon^s \mathrm{d}x = w(x) - w(x_1) - \int_{x_1}^{x} \beta \mathrm{d}x, \tag{9}$$

where x_1 is one node of the beam element. Noting that $w(x) - w(x_1)$ is the actual deflection at point x, while $\int_{x_1}^{x} \beta \mathrm{d}x$ takes into account the displacement due to pure bending, $v(x)$ is named as the "shear gap" to refer to the displacement due to transverse shear deformation. The shear gap is then discretized into nodes

$$v(x) = \sum_{i=1}^{2} N_i \hat{v}_i, \tag{10}$$

where N_i is the shape function and $\hat{v}_i$ is the nodal value of discrete shear gap at node i, which is defined by

$$\hat{v}_i = v(x_i) = \hat{w}_i - \hat{w}_1 - \int_{x_1}^{x_i} \beta \mathrm{d}x. \tag{11}$$

Here $\hat{w}_i = w(x_i)$ and $\hat{w}_1 = w(x_1)$ are the nodal values of deflection at node i and node 1, respectively. The rotation β can also be interpolated from nodal values, hence the discretized form of shear strain is rewritten by

$$\boldsymbol{\varepsilon}^s = \frac{\mathrm{d}v}{\mathrm{d}x} = \mathbf{B}^{DSG} \hat{\mathbf{u}}, \tag{12}$$

where $\hat{\mathbf{u}}$ is the vector of nodal displacements and $\mathbf{B}^{DSG}$ needs to be determined for each type of element.

An application of DSG idea into three-node triangular element (i.e. DSG3 element) would result in an explicit form of $\mathbf{B}^{DSG}$, which only involves the length of element edges and the element area, as can be seen in [9]. In fact for a three-node triangular element, the discrete shear gap at node i can be chosen to be calculated based on either node 1, 2, or 3. The performance of the element is affected by the choice, which is an issue named by "anisotropy" in [10,11]. In order to overcome the issue, a fictitious point located at the center of the triangular element is proposed to be the base-point in [11].

3.2. Formulation of the DSG in four-node quadrilateral element

A direct application of the original formulation of DSG to four-node quadrilateral element, i.e. DSG4 [9], would also be suffered from the same "anisotropy" issue. Hence, in this research, the idea of fictitious point located at the center of the element is adopted. The formulation is presented in details in the followings.

Taking the base-point O into account, the discrete shear gap at node i (one of the four node of a quadrilateral element) can be written similarly to Eq. (11) by

$$\hat{v}_i = \hat{w}_i - w_O - \int_{0}^{l_i} \beta(l) \mathrm{d}l, \tag{13}$$

where the rotation β perpendicular to the line Oi connecting point O and node i can be calculated from the field variables β_x and β_y (see Fig. 1)

$$\beta = \beta_x \cos\alpha_i + \beta_y \sin\alpha_i. \tag{14}$$

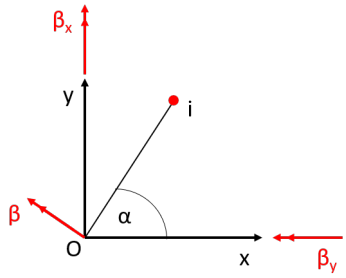

Fig. 1. Rotation β can be calculated from β_x and β_y

The components of shear strain $\boldsymbol{\varepsilon}^s = \left[2\varepsilon_{xz},\ 2\varepsilon_{yz}\right]^T$ are obtained simply by taking the first order derivatives of shear gap v with respect to the x- and y- directions. Within each element, the follow expressions hold

$$\begin{aligned} 2\varepsilon_{xz} = \sum_{i=1}^{4} \frac{\partial N_i}{\partial x}\hat{v}_i = \sum_{i=1}^{4} \frac{\partial N_i}{\partial x}\left[\sum_{j=1}^{4} N_j\left(x_i, y_i\right)\hat{w}_j - \sum_{j=1}^{4} N_j\left(x_O, y_O\right)\hat{w}_j\right] \\ - \sum_{i=1}^{4} \frac{\partial N_i}{\partial x}\left[\int_0^{l_i}\sum_{j=1}^{4} N_j(l)\cos\alpha_i\hat{\beta}_{xj}\mathrm{d}l + \int_0^{l_i}\sum_{j=1}^{4} N_j(l)\sin\alpha_i\hat{\beta}_{yj}\mathrm{d}l\right], \end{aligned} \tag{15}$$

$$\begin{aligned} 2\varepsilon_{yz} = \sum_{i=1}^{4} \frac{\partial N_i}{\partial y}\hat{v}_i = \sum_{i=1}^{4} \frac{\partial N_i}{\partial y}\left[\sum_{j=1}^{4} N_j\left(x_i, y_i\right)\hat{w}_j - \sum_{j=1}^{4} N_j\left(x_O, y_O\right)\hat{w}_j\right] \\ - \sum_{i=1}^{4} \frac{\partial N_i}{\partial y}\left[\int_0^{l_i}\sum_{j=1}^{4} N_j(l)\cos\alpha_i\hat{\beta}_{xj}\mathrm{d}l + \int_0^{l_i}\sum_{j=1}^{4} N_j(l)\sin\alpha_i\hat{\beta}_{yj}\mathrm{d}l\right]. \end{aligned} \tag{16}$$

In the above equations, the approximation within each element has been used, i.e. $\hat{w}_i = \sum_j^4 N_j\left(x_i, y_i\right)\hat{w}_j$, $w_O = \sum_j^4 N_j\left(x_O, y_O\right)\hat{w}_j$, $\beta_x(l) = \sum_j^4 N_j(l)\hat{\beta}_{xj}$ and $\beta_y(l) = \sum_j^4 N_j(l)\hat{\beta}_{yj}$. The compact form similar to Eq. (12) can be written by

$$\boldsymbol{\varepsilon}^s = \begin{bmatrix} 2\varepsilon_{xz} \\ 2\varepsilon_{yz} \end{bmatrix} = \mathbf{B}^{DSG}\hat{\mathbf{u}}, \tag{17}$$

where the vector of nodal displacements is $\mathbf{u} = \left[\hat{w}_1, \beta_{x1}, \beta_{y1}, \hat{w}_2, ..., \hat{w}_4, \beta_{x4}, \beta_{y4}\right]^T$. The matrix $\mathbf{B}^{DSG}$ is calculated as follows

$$\mathbf{B}^{DSG} = \begin{bmatrix} \mathbf{B}_1^{DSG} & \mathbf{B}_2^{DSG} & \mathbf{B}_3^{DSG} & \mathbf{B}_4^{DSG} \end{bmatrix}, \tag{18}$$

where

$$\mathbf{B}_i^{DSG} = \begin{bmatrix} \dfrac{\partial N_i}{\partial x} - N_i^O \sum\limits_{j=1}^{4} \dfrac{\partial N_j}{\partial x} & \dfrac{\partial N_i}{\partial y} - N_i^O \sum\limits_{j=1}^{4} \dfrac{\partial N_j}{\partial y} \\ -\sum\limits_{j=1}^{4} \left(\dfrac{\partial N_j}{\partial x} \cos\alpha_j \int_0^{l_j} N_i(l)\mathrm{d}l \right) & -\sum\limits_{j=1}^{4} \left(\dfrac{\partial N_j}{\partial y} \cos\alpha_j \int_0^{l_j} N_i(l)\mathrm{d}l \right) \\ -\sum\limits_{j=1}^{4} \left(\dfrac{\partial N_j}{\partial x} \sin\alpha_j \int_0^{l_j} N_i(l)\mathrm{d}l \right) & -\sum\limits_{j=1}^{4} \left(\dfrac{\partial N_j}{\partial y} \sin\alpha_j \int_0^{l_j} N_i(l)\mathrm{d}l \right) \end{bmatrix}^T, \quad (19)$$

in which $N_i^O = N_i\left(x_O, y_O\right)$.

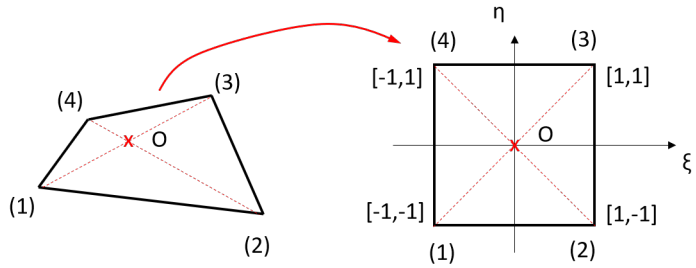

Fig. 2. Transformation of an element from physical space to reference space.

In implementation, the integrals $\int_0^{l_j} N_i(l)\mathrm{d}l$ can be transformed from the physical space into the space of reference element, see Fig. 2. The line integrals in the reference space are pre-computed only once. Therefore, it is efficient to evaluate Eq. (19). The finite element procedure does not change, except that the shear strain components $\boldsymbol{\varepsilon}^s$ are approximated by Eq. (17) instead of Eq. (5), and thus the shear-related component of stiffness matrix is modified, while the bending-related component remains unchanged. Furthermore it is noticed that the following holds in every element

$$\sum_j^4 \frac{\partial N_j(x)}{\partial x} = \sum_j^4 \frac{\partial N_j(x)}{\partial y} = 0. \quad (20)$$

Finally, a stabilization term is introduced into Eq. (8), as recommended by [19]

$$\hat{\mathbf{D}}_s = \frac{\kappa t^3}{t^2 + \alpha h_e^2} \begin{bmatrix} \mu & 0 \\ 0 & \mu \end{bmatrix}, \quad (21)$$

where h_e is the longest side of the element and α is a user-defined positive parameter. For simplicity, α is fixed at 0.1 in this paper.

4. NUMERICAL EXAMPLES

In this section, the performance of the proposed CP-DSG4 element is demonstrated via three numerical examples:

- A patch test.

- A simply supported square plate subjected to uniform pressure.
- A clamped circular plate subjected to uniform pressure.
- A simply supported thin skew plate subjected to uniform pressure.

Properties of CP-DSG4 (e.g. the ability to avoid shear locking, the accuracy in case of mesh distortion and computational efficiency) are investigated, in comparison with other approaches such as Q4 (conventional four-node quadrilateral element), Q4I (Q4 element with selective reduced integration), DSG3 (three-node triangular element with discrete shear gap) [9] and CP-DSG3 (central-point based DSG3) [11]. The well-known MITC4 element [4] is also taken as reference. By DSG3 [9] and CP-DSG3 [11], we mean that those elements are implemented using the explicit formulation presented in the associated documents. Whenever stabilization term Eq. (21) is used, a suffix "stabilized" will be added into the notation. The same isotropic material properties are adopted in all numerical examples: Young's modulus $E = 200$ GPa and Poisson's ratio $\nu = 0.3$.

4.1. Patch test

The patch test is introduced to verify the convergence of the proposed element, CP-DSG4. The patch is given by a simple square plate model being meshed by five quadrilateral elements of irregular shapes, as depicted in Fig. 3. The thickness of the plate is $t = 0.001$ m. The boundary deflection is assumed to be

$$w^{exact} = (1 + x + y + \frac{1}{2}x^2 + xy + \frac{1}{2}y^2) \times 10^{-4} \text{ [m]}. \tag{22}$$

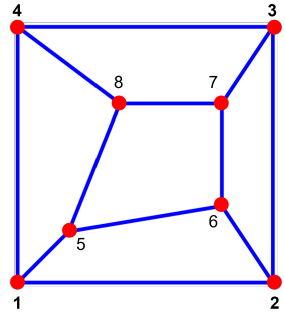

Fig. 3. Meshed model of the patch test. Nodal coordinates are: 1 (0, 0); 2 (0.1, 0.1); 3 (0, 0.1); 4 (0, 0.1); 5 (0.02, 0.02), 6 (0.08, 0.03), 7 (0.08, 0.07), 8 (0.04, 0.07)

The results reported in Table 1 exhibit that the analytical solution is reproduced in the interior nodes. Thus the patch test is passed.

Table 1. Results of interior nodes of the patch test

Node	w	w^{exact}	β_x	β_x^{exact}	β_y	β_y^{exact}
5	0.000104	0.000104	0.000104	0.000104	0.000104	0.000104
6	0.000111	0.000111	0.000111	0.000111	0.000111	0.000111
7	0.000115	0.000115	0.000115	0.000115	0.000115	0.000115
8	0.000111	0.000111	0.000111	0.000111	0.000111	0.000111

4.2. A square plate subjected to uniform pressure

In this example, a square plate of size $a \times a$ with $a = 1$ m subjected to uniform pressure $q = 1\,\mathrm{N/m^2}$ is considered. The maximum deflection, w_c, obtained at the center of the plate is normalized by $\tilde{w} = w_c \cdot 100D_0/(qa^4)$, where $D_0 = Et^3/(12(1-\nu^2))$, with t being the plate thickness. Taking the analytical solution given by Timoshenko and Woinowsky-Krieger [20] as reference, the accuracy of results obtained by CP-DSG4 in regular meshes (i.e. 8×8, 12×12, 16×16, 20×20, 32×32, 48×48 and 64×64 elements) are demonstrated in Fig. 4 for the case that all edges are simply supported (SSSS). Notice that the triangular meshes are achieved by dividing each quadrilateral element into two triangles.

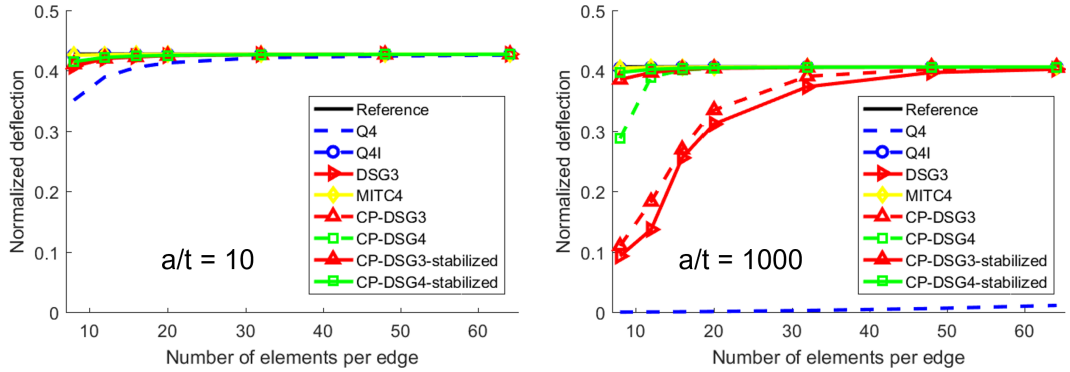

Fig. 4. Numerical results of normalized central deflection obtained by SSSS boundary conditions with two cases: thick plate ($a/t = 10$) and thin plate ($a/t = 1000$)

It is evidently shown that all types of elements considered (i.e. Q4, Q4I, DSG3, MITC4, CP-DSG3 and CP-DSG4) work well in case of thick plate ($a/t = 10$), though Q4 has a little bit less accuracy when the mesh is coarse. For thin plate ($a/t = 1000$), Q4 is unable to deliver reasonable solution due to shear locking, as expected. All the other elements have good performance. The accuracy of CP-DSG4, Q4I and MITC4 are almost equivalent and they outperform both DSG3 and CP-DSG3 in coarse meshes. With simple formulation, Q4I seems to be the most efficient element type for regular mesh. It is also observed that stabilization term is not necessary in thick plate analysis, as the performance of CP-DSG3/CP-DSG4 and their stabilized versions are almost equivalent. For thin plate, stabilization improves accuracy in coarse meshes, especially for triangular elements.

Next, the performance of the elements with discrete shear gap is verified in irregular mesh. The irregular meshes are created from regular meshes by a small perturbation of the nodal positions. An illustration of regular and irregular mesh of 16×16 elements is depicted in Fig. 5. The convergence of central deflection with respect to mesh fineness is exhibited in Fig. 6. It is evidently shown that the Q4I element is severely affected by mesh distortion, while the DSG-enhanced elements are not. Hence it is more reliable to use DSG instead of reduced integration. Among the three types (DSG3, CP-DSG3 and CP-DSG4), CP-DSG4 has the best performance. The accuracy of CP-DSG3 is a little bit better

than that of DSG3. The accuracy of CP-DSG3 can be greatly improved by consideration of stabilization term. Without stabilization, CP-DSG4 is much better than CP-DSG3. For CP-DSG4, stabilization is only really useful in coarse meshes.

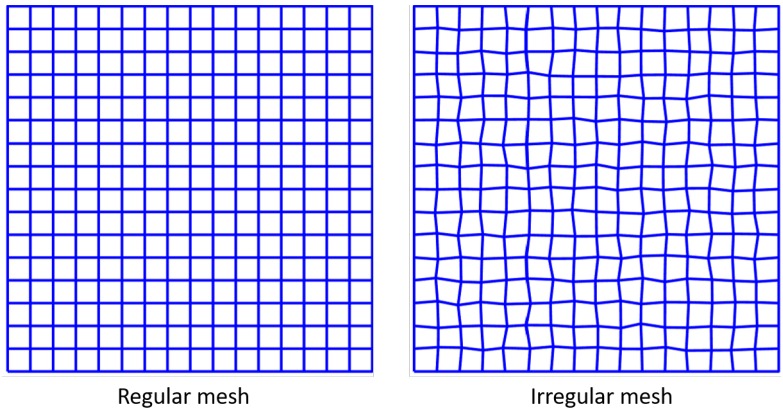

Fig. 5. The regular and irregular meshes of 16×16 quadrilateral elements

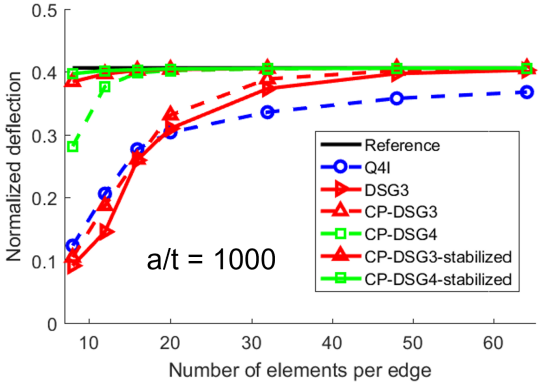

Fig. 6. Numerical results of normalized central deflection obtained by SSSS boundary conditions with thin plate ($a/t = 1000$) and irregular meshes

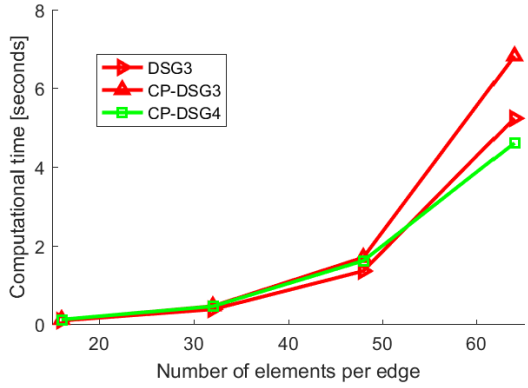

Fig. 7. Computational time with respect to mesh density of the three element types: DSG3, CP-DSG3 and CP-DSG4

Regarding time efficiency, it is obvious that more computational effort is required to calculate the element stiffness matrix of CP-DSG4 than that of DSG3 and CP-DSG3, where the matrices are expressed explicitly. However, given the same number of nodes, the number of triangular elements is much larger than that of quadrilateral elements. The graphs of computational time versus mesh density (represented by number of nodes per edge) are depicted in Fig. 7, clearly demonstrate the efficiency of CP-DSG4. For coarse mesh, elapsed time of CP-DSG4 is higher than that of DSG3 and CP-DGS3, but the difference is not significant. In fine mesh, the computational process would even be faster with CP-DSG4.

4.3. A circular plate subjected to uniform pressure

The performance of the DSG-enhanced elements is further investigated in analysis of a clamped thin circular plate of radius $R = 1$ m being subjected to uniform load $q = 1\,\mathrm{N/m^2}$, as depicted in Fig. 8. The plate thickness is $t = L/500$. Analytical solution of this problem was presented in [21]. For meshing, the circular domain is firstly partitioned into five sub-domains. Each edge is then split into 5, 10, 15, 20 segments in order to generate 125, 500, 1125 and 2000 quadrilateral elements, respectively. The mesh of 125 elements is depicted in Fig. 8. Triangular meshes are obtained by splitting every quadrilaterals into two triangles.

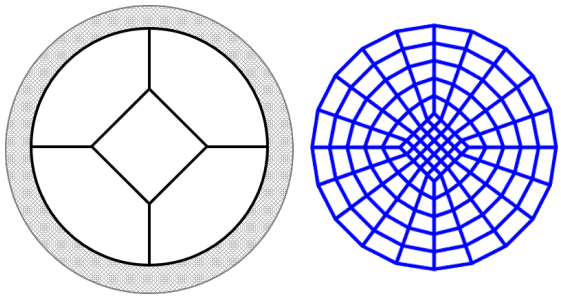

Fig. 8. Sketch of circular plate and the mesh of 125 quadrilateral elements

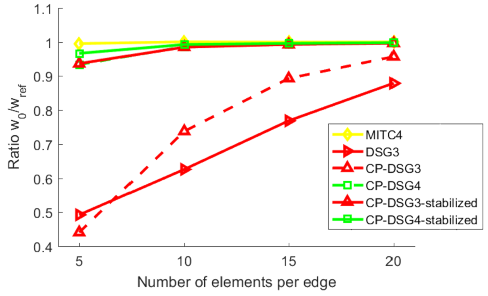

Fig. 9. Convergence of ratio w_0/w_{ref} with respect to mesh density

Denoting w_0 the computed deflection at the center of the plate (which is also the maximum value), and w_{ref} the analytical results, the convergence of ratio w_0/w_{ref} with respect to mesh density is exhibited in Fig. 9. Similarly to the example of square plate in Subsection 4.2, the accuracy of CP-DSG4 is higher than that of CP-DSG3, for the both cases: with and without stabilization. It is clearly observed that in general CP-DSG4 and CP-DSG3 are better than DSG3, even without stabilization. The CP-DSG4 is even equivalent to the stabilized CP-DSG3. The accuracy of CP-DSG4 can be improved by stabilization, especially in the coarsest mesh. MITC4 exhibits good quality in all the meshes being considered. Except for the coarsest mesh, the difference between MITC4 and CP-DSG4/CP-DSG4-stabilized is not significant.

4.4. A skew plate subjected to uniform pressure

In this example, a rhombic plate of side $L = 1$ m with zero deflection ($w = 0$) on boundaries, being subjected to uniform load $q = 1\ \mathrm{N/m^2}$ is investigated, see Fig. 10. This problem is served to study the performance of CP-DSG3, CP-DSG4 and MITC4 in the case of thin plate (thickness is $t = 0.001$ m) with skew geometry. Regular meshes with increasing fineness (8, 12, 16, 20, 32, 48, and 64 elements per edge) are adopted. The normalized central deflection $\tilde{w} = w_c \cdot 1000 D_0/(qL^4) \approx 0.408$ given by Ref. [22] is taken as reference. Results of all the element types being considered tend to converge with respect to mesh fineness. Although the normalized deflections obtained by CP-DSG3 and MITC4 at very coarse meshes (e.g. 8×8, 12×12 and 16×16 elements) are closer to the reference solution, fluctuation in the curves indicates that they are not quite reliable. For

this particular example, performance of CP-DSG4 is slightly better than both CP-DSG3 and MITC4. Both stabilized versions of CP-DSG3 and CP-DSG4 have good agreement with the reference. However, the outcomes of stabilized CP-DSG4 are much closer.

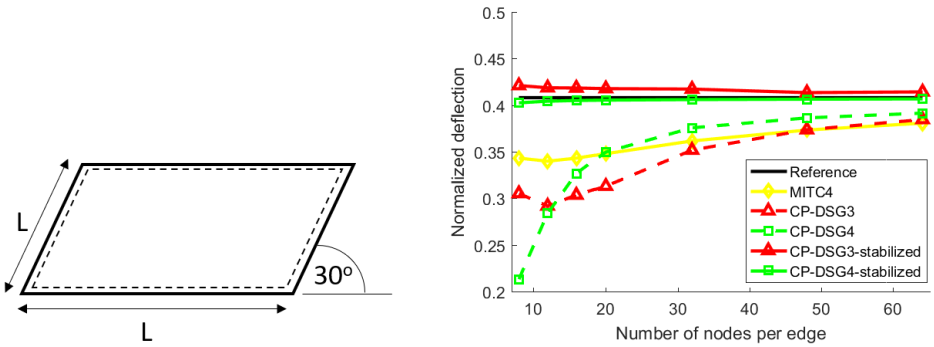

Fig. 10. The skew plate problem: Geometry and numerical results of normalized central deflection

5. CONCLUSION

The central point-based discrete shear gap has been successfully extended into four-point quadrilateral element for analysis of Reissner–Mindlin plates. The followings have been shown:

- The Q4 element is suffered from shear locking, as expected.
- The Q4I is computationally efficient in uniform mesh. However its performance severely deteriorates in case of distorted mesh. The elements with discrete shear gap are not much affected by mesh distortion.
- CP-DSG4 has better accuracy than both DSG3 and CP-DSG3.
- Time efficiency of CP-DSG4 in general is comparable to DSG3 and CP-DSG3. In fine mesh, CP-DSG4 even requires less computational time.

With simple formulation and good performance (in terms of accuracy, time efficiency and immunity to mesh distortion), the CP-DSG4 is a strong candidate for further investigation on plate structures analysis based on Reissner–Mindlin theory.

The authors are aware that a good choice of base-point for DSG4 may lead to an element equivalent to the famous MITC4 [4], as already mentioned in [9]. The performance of CP-DSG4 is almost equivalent to MITC4 in the numerical examples being considered. Furthermore, it is expected that the approach of center-point based discrete shear gap would be extendable for polygonal elements, in which element can take the shape of n-sided polygons. This research has been scheduled for future works.

REFERENCES

[1] T. J. R. Hughes, M. Cohen, and M. Haroun. Reduced and selective integration techniques in finite element analysis of plates. *Nuclear Engineering and Design*, **46**, (1), (1978), pp. 203–222. https://doi.org/10.1016/0029-5493(78)90184-x.

[2] S.-H. Kim and C.-K. Choi. Improvement of quadratic finite element for Mindlin plate bending. *International Journal for Numerical Methods in Engineering*, **34**, (1), (1992), pp. 197–208. https://doi.org/10.1002/nme.1620340112.

[3] D. Wan, D. Hu, S. Natarajan, S. P. A. Bordas, and T. Long. A linear smoothed quadratic finite element for the analysis of laminated composite Reissner-Mindlin plates. *Composite Structures*, **180**, (2017), pp. 395–411. https://doi.org/10.1016/j.compstruct.2017.07.092.

[4] K.-J. Bathe and E. Dvorkin. A four-node plate bending element based on Mindlin/Reissner plate theory and a mixed interpolation. *International Journal for Numerical Methods in Engineering*, **21**, (2), (1985), pp. 367–383. https://doi.org/10.1002/nme.1620210213.

[5] K.-J. Bathe, F. Brezzi, and S. W. Cho. The MITC7 and MITC9 plate bending elements. *Computers & Structures*, **32**, (3-4), (1989), pp. 797–814. https://doi.org/10.1016/0045-7949(89)90365-9.

[6] P. S. Lee and K.-J. Bathe. Development of MITC isotropic triangular shell finite elements. *Computers & Structures*, **82**, (11-12), (2004), pp. 945–962. https://doi.org/10.1016/j.compstruc.2004.02.004.

[7] R. P. R. Cardoso, J. W. Yoon, M. Mahardika, S. Choudry, R. J. A. de Sousa, and R. A. F. Valente. Enhanced assumed strain (EAS) and assumed natural strain (ANS) methods for one-point quadrature solid-shell elements. *International Journal for Numerical Methods in Engineering*, **75**, (2), (2007), pp. 156–187. https://doi.org/10.1002/nme.2250.

[8] L. M. Li, Y. H. Peng, and D. Y. Li. A stabilized underintegrated enhanced assumed strain solid-shell element for geometrically nonlinear plate/shell analysis. *Finite Element Analysis and Design*, **47**, (5), (2011), pp. 511–518. https://doi.org/10.1016/j.finel.2011.01.001.

[9] K.-U. Bletzinger, M. Bischoff, and E. Ramm. A unified approach for shear-locking-free triangular and rectangular shell finite elements. *Computers & Structures*, **75**, (2000), pp. 321–334. https://doi.org/10.1016/s0045-7949(99)00140-6.

[10] P. S. Lee, H.-C. Noh, and K.-J. Bathe. Insight into 3-node triangular shell finite elements: the effects of element isotropy and mesh patterns. *Computers & Structures*, **85**, (7-8), (2007), pp. 404–418. https://doi.org/10.1016/j.compstruc.2006.10.006.

[11] X. Y. Cui and L. Tian. A central point-based discrete shear gap method for plates and shells analysis using triangular elements. *International Journal of Applied Mechanics*, **09**, (2017). https://doi.org/10.1142/s1758825117500557.

[12] S. Shojaee, N. Valizadeh, E. Izadpanah, Q. T. Bui, and T. V. Vu. Free vibration and buckling analysis of laminated composite plates using the NURBS-based isogeometric finite element method. *Composite Structures*, **94**, (5), (2012), pp. 1677–1693. https://doi.org/10.1016/j.compstruct.2012.01.012.

[13] L. Beirao da Veiga, T. J. R. Hughes, J. Kiendl, C. Lovadina, J. Niiranen, A. Reali, and H. Speleers. A locking-free model for Reissner–Mindlin plates: Analysis and isogeometric implementation via NURBS and triangular NURPS. *Mathematical Models and Methods in Applied Sciences*, **25**, (2015), pp. 1519–1551. https://doi.org/10.1142/s0218202515500402.

[14] T. Q. Bui, D. H. Doan, T. V. Do, S. Hirose, and D. D. Nguyen. High frequency modes meshfree analysis of Reissner–Mindlin plates. *Journal of Science: Advanced Materials and Devices*, **1**, (2016), pp. 400–412. https://doi.org/10.1016/j.jsamd.2016.08.005.

[15] T. T. Truong, V. S. Lo, M. N. Nguyen, N. T. Nguyen, and D. K. Nguyen. Evaluation of fracture parameters in cracked plates using an extended meshfree method. *Engineering Fracture Mechanics*, **247**, (2021). https://doi.org/10.1016/j.engfracmech.2021.107671.

[16] H. Nguyen-Xuan, T. Rabczuk, N. Nguyen-Thanh, T. Nguyen-Thoi, and S. P. A. Bordas. A node-based smoothed finite element method with stabilized discrete shear gap technique

for analysis of Reissner-Mindlin plates. *Computational Mechanics*, **46**, (2010), pp. 679–701. https://doi.org/10.1007/s00466-010-0509-x.

[17] J. Videla, S. Natarajan, and S. P. A. Bordas. A new locking-free polygonal plate element for thin and thick plates based on Reissner-Mindlin plate theory and assumed shear strain fields. *Computer & Structures*, **220**, (2019), pp. 32–42. https://doi.org/10.1016/j.compstruc.2019.04.009.

[18] T. Nguyen-Thoi, P. Phung-Van, H. Nguyen-Xuan, and C. Thai-Hoang. A cell-based smoothed discrete shear gap method using triangular elements for static and free vibration analyses of Reissner-Mindlin plates. *International Journal for Numerical Methods in Engineering*, **91**, (7), (2012), pp. 705–741. https://doi.org/10.1002/nme.4289.

[19] M. Lyly, R. Stenberg, and T. Vihinen. A stable bilinear element for the Reissner-Mindlin plate model. *Computer Methods in Applied Mechanics and Engineering*, **110**, (3-4), (1993), pp. 343–357. https://doi.org/10.1016/0045-7825(93)90214-i.

[20] S. Timoshenko and S. Woinowsky-Kriger. *Theory of plates and shells*. McGraw-Hill, (1940).

[21] A. Ayad and A. Rigolot. An improved four-node hybrid-mixed element based upon Mindlin's plate theory. *International Journal for Numerical Methods in Engineering*, **55**, (6), (2002), pp. 705–731. https://doi.org/10.1002/nme.528.

[22] L. S. D. Morley. *Skew plates and structures*. Pergamon Press, (1963).